Vibronic dynamics of Ammonia's $\tilde{D}$ state: supporting information

Max D.J. Waters and Hans Jakob Wörner

1 Computational details

In this study, the calculations are predominantly completed using (time-dependent) density functional theory with the ORCA 4.2.1 program package.[1] For the density functional theory (DFT) and time-dependent DFT (TDDFT) calculations, the calculations were done at the CAM-B3LYP/aug-cc-pVQZ level of theory. Key parameters are compared to coupled-cluster singles, doubles, and perturbative triples (CCSD(T))/aug-cc-pVQZ. All DFT Frequencies reported in Table S4 are calculated using the DFT geometry in Table S2, the CCSD(T) frequencies use the minimum structure shown in Table S3. For anharmonic corrections to the frequencies, these are not possible with ORCA, so Gaussian09 was used.[2] For characterisation of the conical intersection space, OpenMolcas was used because ORCA 4.2.1 does not have the capability to optimise conical intersections between excited states, and the methodology in OpenMolcas is well-documented and fully characterised.[3,4]

2 Optimised structures and frequency comparison

The DFT and TDDFT calculations have been compared to CCSD(T) and EOM-CCSD calculations in a few key areas. In general, the CCSD(T) calculations give an optimised geometry that is closer to the literature parameters than DFT.[5] However, given the higher computational cost and experimental sensitivity, the increased cost (even for such a small system) is not necessary for all calculations. A comparison between the optimised geometric parameters of the $\tilde{X}$ state from the DFT and CCSD(T) calculations is shown in Table S1, and the DFT and CCSD(T) cartesian coordinates are shown in Tables S2 and S3, respectively.

Table S1 Comparison of computed geometric parameters between different levels of theory.

Level-of-theory	NH bond length (Å)	NH_2 bond angle (°)	Pyramidal angle (°)
CAM-B3LYP/aug-cc-pVQZ	1.01127	107.768	37.695
CCSD(T)/aug-cc-pVQZ	1.01280	106.540	39.311
Literature (Herzberg 1966)[5]	1.012	106.67	-

Table S2 Cartesian coordinates (in Å) for the minimum energy geometry of ammonia's $\tilde{X}$ state, calculated at the CAM-B3LYP/aug-cc-pVQZ level of theory.

N	0.000000	0.000000	0.109340
H	0.000000	0.943306	-0.255126
H	0.816927	-0.471653	-0.255126
H	-0.816927	-0.471653	-0.255126

Table S3 Cartesian coordinates (in Å) for the minimum energy geometry of ammonia's $\tilde{X}$ state, calculated at the CCSD(T)/aug-cc-pVQZ level of theory.

N	0.000000	0.000005	0.123783
H	-0.000000	0.937298	-0.259939
H	0.811711	-0.468652	-0.259941
H	-0.811711	-0.468652	-0.259941

In addition to the geometries, the CCSD(T) frequencies do not give better agreement with the experimental values shown Table 1. The anharmonic corrections also do not provide a significant improvement, except for vibrational modes which include stretching motions.

Table S4 A comparison between frequencies at different levels of theory. The Orca 4.2.1 calculations are shown as ORCA, and the Gaussian 09 calculations are shown as G09. Gaussian 09 was used for anharmonic corrections. The DFT calculations are using the CAM-B3LYP functional, and all calculations use an aug-cc-pVQZ basis set.

	$\nu_1(a_1')$	$\nu_2(a_2'')$	$\nu_3(e')$ s	$\nu_3(e')$ a	$\nu_4(e')$ s	$\nu_4(e')$ a
ORCA CCSD(T) (cm^{-1})	3497	1000	3639	3639	1668	1668
ORCA DFT (cm^{-1})	3508	993	3629	3629	1659	1659
G09 DFT (cm^{-1})	3499	1009	3620	3620	1664	1664
G09 DFT (anhar. corr.) (cm^{-1})	3371	899	3405	3400	1619	1562

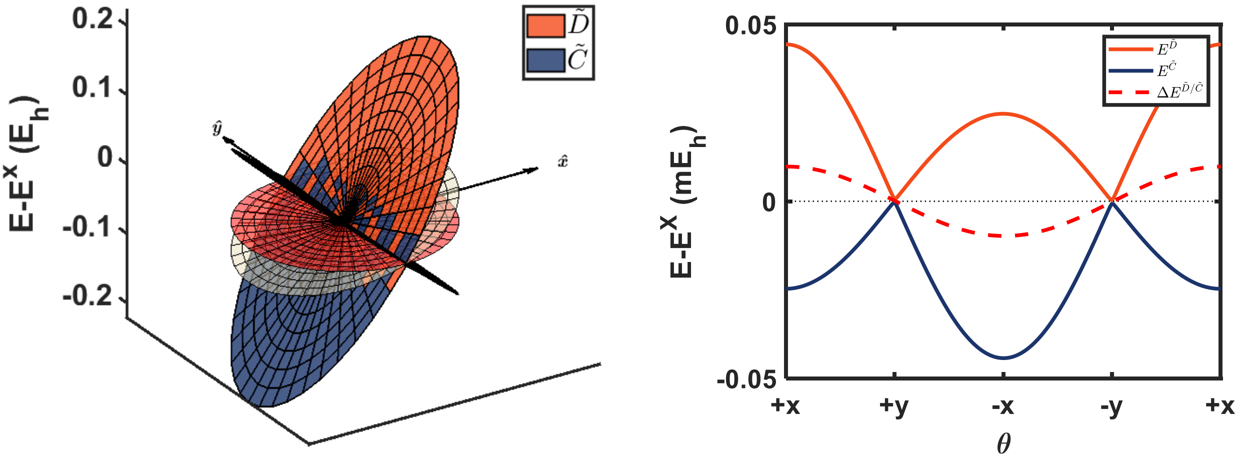

[Hbtp]

Figure S1 The local topography of the conical intersection is shown in three dimensions (left) and two dimensions (right), showing the local energy change of the $\tilde{D}$ and $\tilde{C}$ states, as a function of displacement following the normalised coupling vectors $\hat{x}$ and $\hat{y}$, which are the nonadiabatic coupling mode and the gradient difference mode, respectively. The red circle shows the plane of the intersection, and the white cirlce shows the difference between $\tilde{D}$ and $\tilde{C}$, indicating the path of steepest descent.

3 Calculated thermochemical data

The calculated electronic excitation energies are shown in Table S5, and compared to a measured VUV spectrum.[6] Comparing between EOM-CCSD and TDDFT shows that, in general, TDDFT gives a better agreement with the literature values. For this reason, the potential energy surfaces shown in the main text are calculated at the CAM-B3LYP/aug-cc-pVQZ level of theory.

Table S5 Excitation energy comparison between different levels of theory.

State	CAM-B3LYP/aug-cc-pVQZ (eV)	EOM-CCSD/aug-cc-pVQZ (eV)	Experimental (eV)[6]
$\tilde{A}(\nu_2=0) \leftarrow \tilde{X}(\nu_2=0)$	6.15	6.59	5.72
$\tilde{B}(\nu_2=0) \leftarrow \tilde{X}(\nu_2=0)$	7.51	8.11	7.34
$\tilde{C}(\nu_2=0) \leftarrow \tilde{X}(\nu_2=0)$	7.51	8.11	7.90
$\tilde{D}(\nu_2=0) \leftarrow \tilde{X}(\nu_2=0)$	8.57	9.06	8.65
$\tilde{E}(\nu_2=0) \leftarrow \tilde{X}(\nu_2=0)$	9.35	9.72	9.33

In general, these comparisons between experimental measurements, DFT, and coupled-cluster theory show that the computational approach employed is sufficient to support the experimental photoelectron data. Using more expensive levels of theory, we do not get a significantly better agreement with experimental frequency data, and we get a worse agreement with the electronic energy levels. This could certainly be improved by using a larger basis set (with additional computational cost). However, this is not within the scope of this work.

4 Conical intersection characterisation

The conical intersection (CI), and nonadiabatic coupling (NADC) vectors associated with the crossing, are calculated at the state-averaged complete active space (SA-CASSCF) (6,12)/aug-cc-pVQZ level of theory. The chosen active space included all occupied molecular orbitals (except the nitrogen 1s and nitrogen 2s), with the nine additional orbitals being made up of the A_1 and $A_2\sigma^*$ orbitals, and the $3s$, $3p_x$, $3p_y$, $3p_z$, $3d_{xz}$, $3d_{yz}$, $3d_{z^2}$, and $3d_{x^2-y^2}$ Rydberg orbitals. The local topography is shown in Figure S1. This plot shows that the symmetric wagging motion (the gradient difference vector) efficiently takes the population to the CI region and mediates the crossing.

The dimensionless coupling vectors $\hat{\mathbf{x}}$ and $\hat{\mathbf{y}}$ shown in Figure S1 are normalisations of the nonadiabatic coupling vector and the gradient difference vector (often seen in literature as $\tilde{\mathbf{g}}$ and $\tilde{\mathbf{h}}$)[4], which are calculated as:

$$\hat{\mathbf{x}} = \frac{\tilde{\mathbf{g}}}{\sqrt{\tilde{\mathbf{g}} \cdot \tilde{\mathbf{g}}}} \, ; \quad \hat{\mathbf{y}} = \frac{\tilde{\mathbf{h}}}{\sqrt{\tilde{\mathbf{h}} \cdot \tilde{\mathbf{h}}}} . \tag{1}$$

The characterisation shows that the coupling between the $\tilde{D}$ and $\tilde{C}$ electronic states is a peaked, bifurcating conical intersection. In terms of topography, a peaked conical intersection indicates that the crossing point is the minimum energy point, and are likely to behave as funnels for dynamic processes, directing population to a lower excited state.[4] The bifurcating nature of the intersection seam means that there is more than one pathway that takes the population away from the conical intersection region. This could explain why no vibronic structure is experimentally observed in the $\tilde{C}$ or $\tilde{B}$ state. For ease of reproducibility, the cartesian coordinates for the coupling space, and the displacement vectors are shown in Tables S6,S7, and S8, respectively. The graphical representation of these can be found in the main text in Figure 11.

Table S6 Cartesian coordinates (in Å) for the optimised conical intersection of the crossing between ammonia's $\tilde{D}$ and $\tilde{C}$ states, calculated at the SA-CASSCF(6,12)/aug-cc-pVQZ level of theory.

N	-0.00000493	-0.03078034	-0.17110355
H	-0.00002406	0.97110523	-0.18620090
H	0.95577344	-0.47017843	-0.16321964
H	-0.95574445	-0.47014646	-0.16317592

Table S7 Cartesian displacement coordinates (in Å) following the gradient difference vector ($\hat{\mathbf{x}}$).

N	-0.0002425345792448	-0.2438791848682704	0.0028606672590531
H	-0.0000194648249858	0.0796771140024804	0.0000212856335357
H	0.6786148219674141	0.0819777178912322	-0.0016965165771243
H	-0.6783528359815435	0.0822168435335640	-0.0016664879944054

Table S8 Cartesian displacement coordinates (in Å) following the non-adiabatic coupling vector ($\hat{\mathbf{y}}$).

N	-0.0008023435903256	0.0989679829878423	-0.8189482503100941
H	0.0001375049441773	-0.0194597524389299	0.5558651406003247
H	0.0260668545322181	-0.0410641695708297	0.0534405758178252
H	-0.0254064351441886	-0.0409172841382356	0.0512088794588610

References

[1] F. Neese, *Wiley Interdiscip. Rev.: Comput. Mol. Sci.*, 2018, **8**, e1327.

[2] M. J. Frisch, G. W. Trucks, H. B. Schlegel, G. E. Scuseria, M. A. Robb, J. R. Cheeseman, G. Scalmani, V. Barone, B. Mennucci, G. A. Petersson, H. Nakatsuji, M. Caricato, X. Li, H. P. Hratchian, A. F. Izmaylov, J. Bloino, G. Zheng, J. L. Sonnenberg, M. Hada, M. Ehara, K. Toyota, R. Fukuda, J. Hasegawa, M. Ishida, T. Nakajima, Y. Honda, O. Kitao, H. Nakai, T. Vreven, J. A. Montgomery Jr., J. E. Peralta, F. Ogliaro, M. Bearpark, J. J. Heyd, E. Brothers, K. N. Kudin, V. N. Staroverov, R. Kobayashi, J. Normand, K. Raghavachari, A. Rendell, J. C. Burant, S. S. Iyengar, J. Tomasi, M. Cossi, N. Rega, J. M. Millam, M. Klene, J. E. Knox, J. B. Cross, V. Bakken, C. Adamo, J. Jaramillo, R. Gomperts, R. E. Stratmann, O. Yazyev, A. J. Austin, R. Cammi, C. Pomelli, J. W. Ochterski, R. L. Martin, K. Morokuma, V. G. Zakrzewski, G. A. Voth, P. Salvador, J. J. Dannenberg, S. Dapprich, A. D. Daniels, ö. Farkas, J. B. Foresman, J. V. Ortiz, J. Cioslowski and D. J. Fox, *Gaussian09 Revision E.01*.

[3] I. Fdez. Galván, M. Vacher, A. Alavi, C. Angeli, F. Aquilante, J. Autschbach, J. J. Bao, S. I. Bokarev, N. A. Bogdanov, R. K. Carlson, L. F. Chibotaru, J. Creutzberg, N. Dattani, M. G. Delcey, S. S. Dong, A. Dreuw, L. Freitag, L. M. Frutos, L. Gagliardi, F. Gendron, A. Giussani, L. González, G. Grell, M. Guo, C. E. Hoyer, M. Johansson, S. Keller, S. Knecht, G. Kovačević, E. Källman, G. Li Manni, M. Lundberg, Y. Ma, S. Mai, J. P. Malhado, P. Å. Malmqvist, P. Marquetand, S. A. Mewes, J. Norell, M. Olivucci, M. Oppel, Q. M. Phung, K. Pierloot, F. Plasser, M. Reiher, A. M. Sand, I. Schapiro, P. Sharma, C. J. Stein, L. K. Sørensen, D. G. Truhlar, M. Ugandi, L. Ungur, A. Valentini, S. Vancoillie, V. Veryazov, O. Weser, T. A. Wesołowski, P. O. Widmark, S. Wouters, A. Zech, J. P. Zobel and R. Lindh, *OpenMolcas: From Source Code to Insight*, 2019.

[4] I. Fdez. Galván, M. G. Delcey, T. B. Pedersen, F. Aquilante and R. Lindh, *J. Chem. Theory Comput.*, 2016, **12**, 3636–3653.

[5] G. Herzberg, *Electronic Spectra and Electronic Structure of Polyatomic Molecules*, Van Nostrand, 1966.

[6] P. Limão-Vieira, N. C. Jones, S. V. Hoffmann, D. Duflot, M. Mendes, A. I. Lozano, F. Ferreira Da Silva, G. García, M. Hoshino and H. Tanaka, *J. Chem. Phys.*, 2019, **151**, 184302.